In vivo molecular imaging of myocardial angiogenesis using the $\alpha_v\beta_3$ integrin-targeted tracer ^{99m}Tc-RAFT-RGD

Julien Dimastromatteo, MS,[a,b,d] Laurent M. Riou, PhD,[a,b] Mitra Ahmadi, PharmD,[a,b] Guillaume Pons, MS,[a,b] Eric Pellegrini, PhD,[a,b,e] Alexis Broisat, PhD,[a,b] Lucie Sancey, PhD,[a,b] Tatiana Gavrilina, MD,[a,b] Didier Boturyn, PhD,[b,c] Pascal Dumy, PhD,[b,c] Daniel Fagret, MD, PhD,[a,b] and Catherine Ghezzi, PhD[a,b]

Background. **Myocardial angiogenesis following reperfusion of an infarcted area may impact on patient prognosis and pro-angiogenic treatments are currently evaluated. The non-invasive imaging of angiogenesis would therefore be of potential clinical relevance in these settings. ^{99m}Tc-RAFT-RGD is a novel ^{99m}Tc-labeled tracer that targets the $\alpha_v\beta_3$ integrin. Our objective was to determine whether this tracer was suitable for myocardial angiogenesis imaging.**

Methods and Results. **A rat model of reperfused myocardial infarction was employed. Fourteen days following reperfusion, the animals were injected with ^{99m}Tc-RAFT-RGD or with its negative control ^{99m}Tc-RAFT-RAD. Fourteen animals were dedicated to autoradiographic imaging, infarct staining, and gamma-well counting of myocardial activity. In vivo dual-isotope pinhole SPECT imaging of ^{201}Tl and ^{99m}Tc-RAFT-RGD or ^{99m}Tc-RAFT-RAD was also performed in 11 additional animals. Neovessels were observed by immunostaining in the infarcted and peri-infarct areas. ^{99m}Tc-RAFT-RGD infarct-to-normal ratios by gamma-well counting and ex vivo imaging (2.5 ± 0.6 and 4.9 ± 0.9, respectively) were significantly higher than those of ^{99m}Tc-RAFT-RAD (1.7 ± 0.2 and 2.2 ± 0.4, respectively, $P < .05$). The infarcted area was readily visible in vivo by SPECT with ^{99m}Tc-RAFT-RGD but not with ^{99m}Tc-RAFT-RAD (infarct-to-normal zone activity ratio, 2.5 ± 0.6 and 1.7 ± 0.4, respectively, $P < .05$).**

Conclusion. **^{99m}Tc-RAFT-RGD allowed the experimental in vivo molecular imaging of myocardial angiogenesis. (J Nucl Cardiol 2010;17:435–43.)**

Key Words: Molecular imaging • angiogenesis • radiopharmaceuticals • biodistribution

Cardiovascular diseases are the leading cause of mortality worldwide.[1] In the United States, myocardial infarction (MI) is the main entity responsible for cardiovascular mortality, with 875,000 events/year. In 22% of men and 46% of women, MI leads to the development of heart failure (HF) within 6 years, and 80% and 70% of male and female HF patients will die within 8 years.[2]

Myocardial infarction is characterized by myocyte necrosis and apoptosis leading to scar formation, left ventricular dilatation, and remodeling which may ultimately evolve into HF.[3,4] In the acute phase of MI, reperfusion of the infarcted area results in intense inflammatory processes.[5] Angiogenesis, i.e., the formation of new blood vessels from an existing vascular network,[6] is triggered by the inflammatory process to provide the healing infarcted myocardium with oxygen and nutrients necessary to sustain the high metabolism in the area subjected to inflammation and scar formation.[5]

Experimentally, techniques such as stem cell injection, gene transfer, growth factor, or pharmacologic

From the INSERM, U877, Radiopharmaceutiques Biocliniques, Faculté de Médecine de Grenoble,[a] La Tronche, Grenoble, France; Université Joseph Fourier,[b] Grenoble, France; Département de Chimie Moléculaire,[c] CNRS, UMR-5250, Grenoble, France; ERAS Labo,[d] Saint Nazaire les Eymes, France; Biospace Lab,[e] Paris, France.

Funding: Financial support was provided by the National Institute for Health and Medical Research (INSERM), the National Agency for Research and technology (ANRT), and ERAS Labo. The authors have no conflict of interest to disclose.

Received for publication Apr 28, 2009; final revision accepted Dec 25, 2009.

Reprint requests: Laurent M. Riou, PhD, INSERM U877, Radiopharmaceutiques Biocliniques, Faculté de Médecine de Grenoble, 38700 La Tronche, Grenoble, France; *Laurent.Riou@ujf-grenoble.fr.*

1071-3581/$34.00

doi:10.1007/s12350-010-9191-9

treatments have succeeded at inducing angiogenesis, improving tissue perfusion, and enhancing cardiac function following reperfused MI.[7-15] Therefore, it has been hypothesized that the amplitude of the angiogenic phenomenon may impact on patient prognosis. Although initial clinical studies yielded encouraging results, subsequent controlled trials generated more controversial data.[13,16,17] In addition to its potential for the prognostic evaluation of patients, there is a need for a non-invasive tool allowing the assessment of the efficacy of pro-angiogenic treatments.[18]

Cell-cell and cell-matrix interactions are performed by endothelial cells during angiogenesis. These interactions are mediated by integrins, and heterodimeric receptor family composed of α and β transmembraneous subunits. Specifically, $\alpha_V\beta_3$ integrin plays a major role in angiogenesis since it is specifically overexpressed on the surface of newly formed endothelium.[19] The cyclic Arg-Gly-Asp (cRGD) peptidic sequence specifically binds to the $\alpha_V\beta_3$ integrin[20] and has been shown to allow tumoral angiogenesis imaging in vivo following ^{18}F or ^{99m}Tc radiolabeling.[21,22]

Regioselectivity Addressable Functionalized Template-RGD (RAFT-RGD) is a novel compound composed of four cyclo(RGDfK) sequences tethered on a cyclodecapeptide that specifically binds to the $\alpha_V\beta_3$ integrin.[23] ^{99m}Tc-RAFT-RGD has previously been validated in vivo by Sancey et al[24] as a tracer of tumoral angiogenesis. The authors have also recently shown that multimeric RGD molecules are co-internalized with the receptor, suggesting increased affinity of the peptide scaffold for the $\alpha_V\beta_3$ integrin.[25] The aim of the present study was to determine whether ^{99m}Tc-RAFT-RGD would allow the non-invasive imaging of angiogenesis following experimental MI.

METHODS

Tracers

Synthesis. RAFT(cyclo[-RGDfK-])$_4$ (RAFT-RGD) and the negative control RAFT(cyclo[-RADfK-])$_4$ (RAFT-RAD) were synthesized as previously described.[23]

Labeling. ^{125}I labeling was performed by adding 20 to 50 μg of RAFT-RGD or RAFT-RAD to 10 μL of chloramin-T at 5 mg/mL (Amersham Pharmacia, Meylan, France) and ~18.5 MBq of ^{125}I. After 20 minutes, the oxidation was stopped using 40 μL of sodium pyrosulfite (4 mg/mL). The radiochemical purity (RCP) was determined using thin-layer chromatography (TLC) using RP-18 TLC plates and acetonitrile/H_2O (35/65) as the eluant. RCP was ≥95%. ^{99m}Tc labeling of RAFT-RGD and RAFT-RAD was performed as previously described.[24] Radiochemical purity was ≥97%.

In Vitro Experiments

Cell culture. HMVEC (#CC-2517 Cambrex, Emerainville, France) were cultured with EGM-2-MV® BulletKit® (Cambrex).

Cellular uptake. ^{125}I-RAFT-RGD or ^{125}I-RAFT-RAD of 3.5, 7, 15, or 30 nmol were incubated for 30 min prior to cell rinsing with PBS and lysis using SDS 1%. Tracer uptake was determined by gamma-well counting (Cobra II Packard) and proteins were quantified using the modified-Lowry method.

Competition. HMVECs were incubated for 30 min in the presence of 2.2 nmol of ^{125}I-RAFT-RGD and in the absence or presence of 215 nmol of unlabeled cRGD. Tracer uptake was then determined as described above.

In Vivo Experiments

All experiments were approved by the Animal Care and Use Committee of the Military Research and Health Center (CRSSA, authorization # 2006/37.0), Grenoble, France.

Experimental induction of myocardial angiogenesis in rats. Male Wistar rats (n = 32; mean weight, 399 ± 9 g) were used (Charles River Laboratories, France). The anesthesia was induced using an intraperitoneal injection of ketamine (10 wt/vol.%) and xylazine (2 wt/vol.%). The animals were then intubated and ventilated (Harvard, model 683) and the anesthesia was maintained with isoflurane (1.5%). A left thoracotomy was performed and a snare ligature was placed around the left anterior descending coronary artery and tightened using a 5/0 suture for 45 min before reperfusion. The chest was closed (#2 Tevdek suture, Deknatel, Fall River, MA) and isoflurane inhalation was discontinued. The cannula was removed as soon as the animals were able to breathe spontaneously.

Imaging of myocardial angiogenesis. Fourteen days following MI and reperfusion, the animals were re-anesthetized as described above and divided into two experimental groups. Group 1 animals were initially performed in order to provide ex vivo proof-of-concept that ^{99m}Tc-RAFT-RGD was suitable for the assessment of myocardial angiogenesis. Based on the positive results from Group 1, Group 2 animals were used for the evaluation of the potential of ^{99m}Tc-RAFT-RGD for the in vivo imaging of myocardial angiogenesis.

Group 1: Ex vivo imaging and biodistribution. Group 1 animals (n = 21) were dedicated to the evaluation of ^{99m}Tc-RAFT-RGD angiogenesis imaging feasibility. The right saphenous vein was exposed for ^{99m}Tc-RAFT-RGD (96 ± 11 MBq; n = 11) or ^{99m}Tc-RAFT-RAD (107 ± 30 MBq; n = 3) injection. The animals were euthanized 60 min following injection with an overdose of pentobarbital. Samples of blood and organs were then immediately excised, quickly rinsed, and weighed for gamma-well counting. The 60 min time point was chosen based on ^{99m}Tc-RAFT-RGD blood activity determination at 1, 5, 10, 30, 60, 90, and 120 min following intravenous injection of the tracer (40.1 ± 4.3 MBq, n = 3). Indeed, ^{99m}Tc-RAFT-RGD cleared

from the blood in a biexponential manner with an initial, fast decrease ($T_{1/2\alpha} = 2.6$ min). Tracer activity then remained relatively stable between 20 and 120 min following injection ($T_{1/2\beta} = 230$ min). Four additional animals from Group 1 were dedicated to CD31 and $\alpha_V\beta_3$ immunostaining.

Post-mortem analysis: *Immunohistochemistry and histology* Following euthanasia, the myocardium was excised, quickly rinsed, and snap-frozen in methylbutane. Six micrometer thick short-axis sections were obtained (Microm HM 505 E cryotome, Francheville, France) and fixed in acetone for 2 min before air-drying for ~1 h. Immunostaining of vascular cells, neovessels and macrophages was performed using an anti-CD31 monoclonal antibody (1/25, BD Biosciences, ref. #550300), an anti-$\alpha_V\beta_3$ monoclonal antibody (1/50, AbCAM, ref. #ab7166), or an anti-KiM2R (1/400, BMA Biomedicals, ref. #T-3004), respectively, with standard protocols. Twenty micrometer thick slices adjacent to those used for immunohistochemistry were incubated for 15 min at 37°C in a Nitroblue Tetrazolium (NBT) solution (0.04% in 0.05 M sodium succinate buffer, pH 7.6) to delineate the infarcted tissue. Tissue counterstain was performed using hematoxylin.

Biodistribution Samples of infarcted and normal myocardium, lung, liver, spleen, kidney, skeletal muscle, and blood were obtained and weighted prior to gamma-well counting with a 122-160 keV window (Cobra II, Packard Instruments, Rungis, France). Tissue counts were corrected for background and decay. The activity was normalized to the injected dose (ID) and wet tissue weight and expressed as %ID/g.

Autoradiography and infarct staining Heart samples were embedded in optimal cutting temperature compound. Twenty micrometer thick short-axis slices were used for autoradiographic imaging (n = 3/animal) using a β-imager (Biospace Mesures, Paris, France). Twenty micrometer thick slices adjacent to those used for autoradiographic imaging were used for NBT infarct staining as described above and digitalized (CanoScan 4200F, Canon). The infarct size area was quantified using ImageJ software (NIH) and expressed as percent of the total left ventricular area (% LV). This value was used for comparison purposes with the area of ^{99m}Tc-RAFT-RGD or ^{99m}Tc-RAFT-RAD myocardial uptake as determined on the adjacent slice.

Analysis and quantification of ex vivo autoradiographic images Autoradiographic images were analyzed by a blinded observer using β-vision$^+$ software (Biospace Mesures). Regions of Interest (ROIs) were drawn in the normal, peri-infarct and central infarcted areas as identified from NBT infarct staining and tracer uptake was expressed as counts/min/mm^2. Autoradiographic images were also used for the quantification of tracer uptake area expressed as % LV.

Group 2: In vivo SPECT imaging. Group 2 animals (n = 11) were dedicated to in vivo imaging of angiogenesis with ^{99m}Tc-RAFT-RGD. The saphenous vein was exposed for ^{201}Tl (37 ± 1 MBq, n = 11) and ^{99m}Tc-RAFT-RGD (135 ± 6 MBq, n = 6) or ^{99m}Tc-RAFT-RAD (143 ± 7 MBq, n = 5) simultaneous bolus injections. Thirty minutes following tracer injections, a 60 minutes in vivo dual-isotope myocardial SPECT acquisition was started. A small animal imaging camera with a 1 mm pinhole collimator was used (Gamma-imager S, Biospace Mesures, Paris, France). The window settings were 125-150 keV and 55-85 keV for ^{99m}Tc and ^{201}Tl, respectively. The animals were euthanized at the end of the acquisition as described above.

Analysis and quantification of in vivo tomographic images: Image reconstruction was performed using γ-acquisition software. Image processing was performed in Amira software. Consecutive short-axis slices were generated from base to apex. These 2D, dual-isotope extracted slices were analyzed by a blinded observer using γ-vision$^+$ software (Biospace Mesures). ^{201}Tl, ^{99m}Tc-RAFT-RGD or ^{99m}Tc-RAFT-RAD activity was quantified in infarcted, thallium negative and normal, thallium positive myocardial areas and ^{201}Tl, ^{99m}Tc-RAFT-RGD and ^{99m}Tc-RAFT-RAD infarct-to-normal activity ratios were computed.

Statistical Analysis

Values are presented as mean ± SD. Statistical computations were performed using SYSTAT software (SPSS, Inc.). Between-groups comparisons were performed using unpaired *t*-test whereas within-group analysis was performed using one-way analysis of variance. *P* values <.05 were considered statistically significant.

RESULTS

In Vitro Experiments

The results are presented in Figure 1. There was a significant 3.3-fold higher radiolabeled RAFT-RGD uptake on HMVECs when compared to that of RAFT-RAD at all concentrations tested (Figure 1a). In addition, competition experiments indicated that radiolabeled RAFT-RGD uptake was inhibited by 60% in the presence of a 200-fold excess of unlabeled cRGD (Figure 1b).

CD31, $\alpha_V\beta_3$, and KiM2R Immunostaining

Results from CD31, $\alpha_V\beta_3$, and KiM2R immunostaining are presented in Figure 2. Endothelial CD31 expression was observed in the normal as well as in the peri-infarct and infarcted areas (Figure 2b, f, j) as identified using NBT staining (Figure 2a). $\alpha_V\beta_3$ immunostaining was observed in the infarcted and peri-infarct zones, but not in the remote myocardium (Figure 2c, g, k). Macrophage KiM2R expression was observed in the peri-infarct zone only (Figure 2d, h, l). Specificity of the immunostaining was confirmed by the lack of staining in the absence of the primary antibody (Figure 2e, i, m).

^{99m}Tc-RAFT-RGD and ^{99m}Tc-RAFT-RAD Biodistributions (Group 1)

The biodistributions of ^{99m}Tc-RAFT-RGD and ^{99m}Tc-RAFT-RAD are presented in Table 1. ^{99m}Tc-RAFT-RGD excretion mainly occurred through the

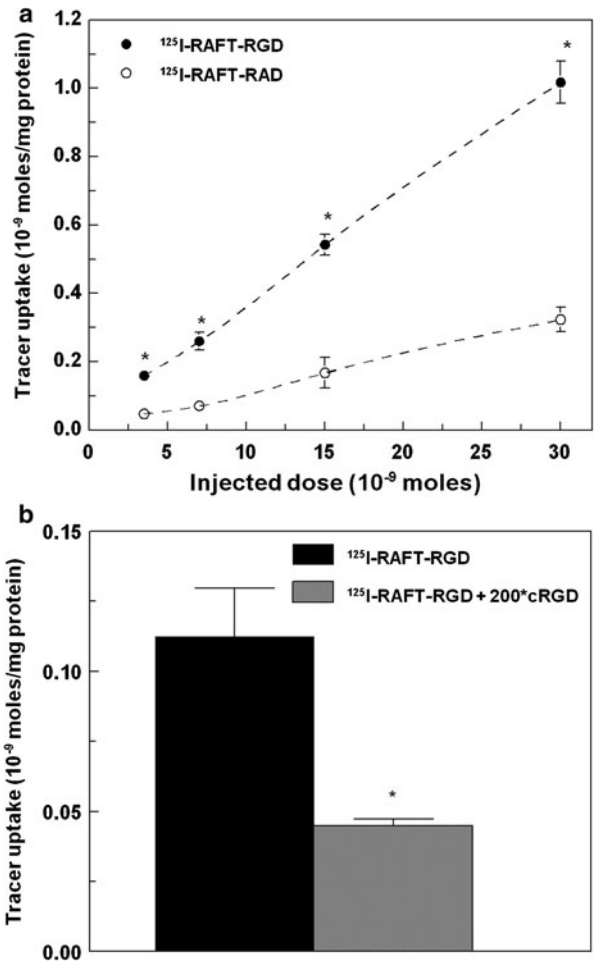

Figure 1. a Thirty minutes ^{99m}Tc-RAFT-RGD and ^{99m}Tc-RAFT-RAD cellular uptake on human microvascular endothelial cells (HMVECs) as a function of tracer concentration. * $P < .01$ vs. ^{99m}Tc-RAFT-RAD; **b** 30-minutes ^{99m}Tc-RAFT-RGD cellular uptake on HMVECs in the absence or presence of a 200-fold excess of cRGD. * $P < .01$ vs. ^{99m}Tc-RAFT-RGD.

kidneys whereas the elimination of ^{99m}Tc-RAFT-RAD mainly involved the hepatic route. The lung, liver, and skeletal muscle uptakes of ^{99m}Tc-RAFT-RGD and ^{99m}Tc-RAFT-RAD were not significantly different, whereas ^{99m}Tc-RAFT-RGD circulating blood activity was significantly lower than that of ^{99m}Tc-RAFT-RAD. Similar activities of ^{99m}Tc-RAFT-RGD and ^{99m}Tc-RAFT-RAD were observed in the normal myocardial area (0.17 ± 0.07 vs. 0.18 ± 0.01%ID/g, respectively, P = NS), whereas ^{99m}Tc-RAFT-RGD activity was significantly higher than that of ^{99m}Tc-RAFT-RAD in the infarcted area (0.42 ± 0.16 vs. 0.30 ± 0.05%ID/g, respectively, $P < .05$). In addition, the infarct-to-normal zone ^{99m}Tc-RAFT-RGD activity ratio was significantly higher than that of ^{99m}Tc-RAFT-RAD (2.5 ± 0.6 vs. 1.7 ± 0.2, respectively, $P < .01$) (Table 2).

Imaging of Myocardial Angiogenesis with ^{99m}Tc-RAFT-RGD

Ex vivo autoradiographic imaging (Group 1). Figure 3 shows representative autoradiographic images (bottom panels) and the corresponding NBT infarct staining (upper panels). ^{99m}Tc-RAFT-RGD uptake was readily observed as a hot spot in the reperfused antero-septal area corresponding to the infarcted area as delineated by NBT staining with little tracer activity in the normal area. ^{99m}Tc-RAFT-RGD uptake was also observed in the peri-infarct area. In comparison to that of ^{99m}Tc-RAFT-RGD, the uptake of ^{99m}Tc-RAFT-RAD in the reperfused area was lower in size and magnitude, and no tracer uptake occurred in the peri-infarct area (Figure 3).

Quantification of autoradiographic and NBT infarct staining images indicated that mean ^{99m}Tc-RAFT-RGD peri-infarct-to-normal (P/N) as well as infarct-to-normal (I/N) zone activity ratios were significantly higher than that of ^{99m}Tc-RAFT-RAD (P/N ratios, 1.7 ± 0.5 vs. 1.1 ± 0.2, I/N ratios, 4.9 ± 0.9 vs. 2.2 ± 0.4, respectively, $P < .001$) (Table 2). Moreover, there was a strong trend towards a significantly smaller ^{99m}Tc-RAFT-RAD uptake area when compared to that of ^{99m}Tc-RAFT-RGD (11.5 ± 5.8 vs. 22.0 ± 1.1% LV, respectively, $P = .06$) in the presence of similar infarct sizes (18.6 ± 7.8 vs. 19.6 ± 5.0% LV for animals injected with ^{99m}Tc-RAFT-RAD and ^{99m}Tc-RAFT-RGD, respectively, $P = .88$).

In vivo dual-isotope SPECT imaging (Group 2). Representative myocardial short-axis serial slices from the same animal following in vivo dual-isotope pinhole SPECT imaging of ^{201}Tl and ^{99m}Tc-RAFT-RGD or ^{99m}Tc-RAFT-RAD are presented in Figure 4. The ^{201}Tl perfusion defect delineated the infarcted area in which a robust uptake of ^{99m}Tc-RAFT-RGD was consistently observed in comparison to the normal zone. On the opposite, no preferential ^{99m}Tc-RAFT-RAD uptake occurred in the infarcted area and tracer activity mainly originated from the LV cavity. Image quantification indicated that the ^{201}Tl infarct-to-normal zone ratios were similar in animals injected with ^{99m}Tc-RAFT-RGD or ^{99m}Tc-RAFT-RAD (0.4 ± 0.1 and 0.4 ± 0.1, respectively, P = NS) whereas the ^{99m}Tc-RAFT-RGD infarct-to-normal zone ratio was significantly higher than the ^{99m}Tc-RAFT-RAD ratio (2.5 ± 0.6 vs. 1.7 ± 0.4, respectively, $P < .05$) (Table 2).

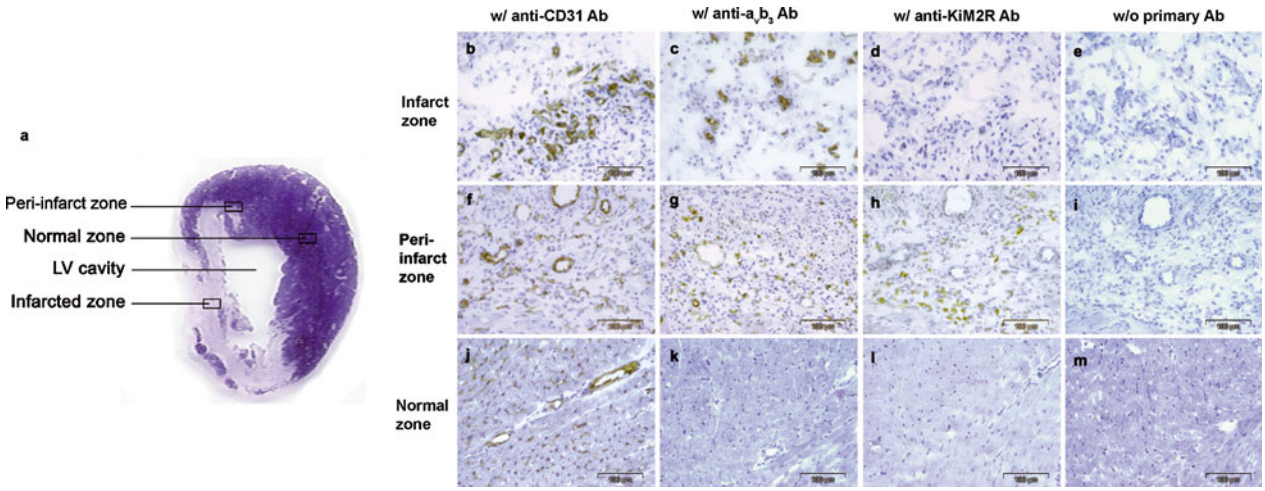

Figure 2. (**a**) NBT staining of the infarcted (*white*) and normal (*purple*) areas from a short-axis myocardial section. Inserts indicate the location of the infarcted, peri-infarct, and normal areas magnified in panels (**b**) through (**m**) in order to illustrate results from immunostaining experiments. CD31 expression was observed in the infarcted (**b**) as well as in the peri-infarct (**f**) and normal (**j**) zones, indicating the presence of vessels in these areas. Panels (**c**), (**g**), and (**k**) indicate that $\alpha_V\beta_3$ expression was observed in the infarcted and peri-infarct zones but not in the normal area. KiM2R positive immunostaining was observed exclusively in the peri-infarct zone (**h**) when compared with the infarcted (**d**) and normal areas (**l**). Specificity of immunostaining experiments was demonstrated by the lack of staining in the absence of the primary antibody (**e**, **i**, **m**).

Table 1. Organ biodistribution of ^{99m}Tc-RAFT-RGD and ^{99m}Tc-RAFT-RAD at 60 minutes following tracer injection

Organs	^{99m}Tc-RAFT-RGD	^{99m}Tc-RAFT-RAD
Lung	0.40 ± 0.14	0.40 ± 0.02
Liver	0.64 ± 0.19	1.20 ± 0.13
Spleen	0.40 ± 0.21*	0.23 ± 0.00
Kidney	4.74 ± 0.34*	0.23 ± 0.02
Skeletal muscle	0.09 ± 0.03	0.11 ± 0.05
Blood	0.36 ± 0.20*	0.61 ± 0.05
Myocardium		
Infarcted zone	0.42 ± 0.16*†	0.30 ± 0.05†
Normal zone	0.17 ± 0.07	0.18 ± 0.01

Values are expressed as %ID/g. *$P < .05$ vs. ^{99m}Tc-RAFT-RAD; $^{\dagger}P < .05$ vs. normal zone.

DISCUSSION

The clinical importance of non-invasive angiogenesis assessment was recently emphasized in a pilot imaging study on patients.[26] In the present study, experimental myocardial ischemia resulted in the induction of angiogenesis in the infarcted and peri-infarct zones at day 14 following reperfusion as previously described by others[27] and as demonstrated by positive CD31 and $\alpha_V\beta_3$ immunostaining in the infarcted and peri-infarct zones. In addition to neovessels, macrophages are also known to express the $\alpha_V\beta_3$ integrin.[28] However, macrophage KiM2R positive immunostaining was exclusively observed in the peri-infarct zone. $\alpha_v\beta_3$ integrin expression in the infarcted area therefore mainly originated from neovessels in our experimental conditions. Peak tissue accumulation of macrophages was observed by Sun et al[29] at day 7 following myocardial infarction and declined thereafter whereas experiments were performed at day 14 following infarction in the present study. Moreover, Higuchi et al[30] recently demonstrated that the myocardial uptake of the PET agent [^{18}F]-galacto-RGD correlated with vascular density but

Table 2. Mean tracer activity ratios from gamma-well counting of myocardial samples, ex vivo autoradiographic and in vivo SPECT image quantification

Groups	^{99m}Tc-RAFT-RGD	^{99m}Tc-RAFT-RAD
Gamma-well counting, I/N	2.54 ± 0.64**	1.69 ± 0.16
Autoradiography, I/N	4.93 ± 0.95***	2.18 ± 0.37
Autoradiography, P/N	1.74 ± 0.50*	1.09 ± 0.15
In vivo imaging (I/N)		
^{99m}Tc-labeled	2.45 ± 0.63*	1.66 ± 0.35
^{201}Tl	0.36 ± 0.07	0.37 ± 0.12

P/N, Peri-infarct-to-normal tracer activity ratio; *I/N*, infarct-to-normal tracer activity ratio.
Values are expressed as %ID/g. *$P < .05$ vs. ^{99m}Tc-RAFT-RAD, **$P < .01$ vs. ^{99m}Tc-RAFT-RAD, ***$P < .001$ vs. ^{99m}Tc-RAFT-RAD.

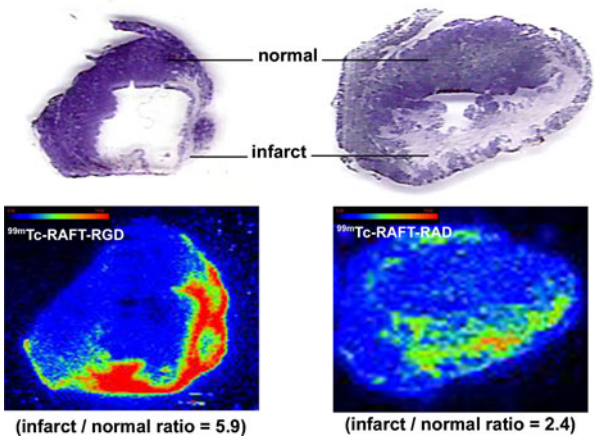

Figure 3. Representative NBT infarct staining of short-axis myocardial slices (*upper panels*) and corresponding autoradiographic images of ^{99m}Tc-RAFT-RGD (*left*) and ^{99m}Tc-RAFT-RAD (*right*) uptake on adjacent slices from the same animals (*lower panels*). Individual infarct-to-normal zone ratios are indicated in parenthesis.

not with the amplitude of macrophage infiltration in a similar rat model of reperfused myocardial infarction, suggesting that angiogenesis represents the main source for $\alpha_V\beta_3$ expression in this setting.

The cRGD sequence binds specifically to the $\alpha_V\beta_3$ integrin.[20] Moreover, multimeric RGD-containing tracers display an improved integrin affinity.[31] The ^{99m}Tc-RAFT-RGD tracer evaluated in the present study contains 4 cRGD bound onto a cyclodecapeptidic scaffold (RAFT) and labeled with ^{99m}Tc.[23] The specificity of RAFT-RGD binding to the $\alpha_V\beta_3$ integrin compared to RAFT-RAD or to the $\alpha_V\beta_5$ and $\alpha_V\beta_1$ integrins has been demonstrated previously.[32] A recent study indicated that although integrins are known to present at least two affinity states on live cells, a single Kd value was observed for RAFT-RGD-Cy5, suggesting that the tracer bound almost exclusively to $\alpha_V\beta_3$ integrins in the active state.[25] In addition, in vitro results from the present study confirmed that RAFT-RGD specificity for the $\alpha_V\beta_3$ integrin was maintained following radiolabeling of the tracer, as demonstrated by experiments indicating a significantly higher uptake of RAFT-RGD than RAFT-RAD in HMVEC cells expressing the $\alpha_V\beta_3$ integrin[33] and a significant inhibition of radiolabeled RAFT-RGD cellular binding in the presence of an excess of unlabeled cRGD. Moreover, ^{99m}Tc-RAFT-RGD was previously and successfully employed to image $\alpha_V\beta_3$ tumoral expression in mouse by SPECT imaging.[24]

In the present study, ^{99m}Tc-RAFT-RGD and ^{99m}Tc-RAFT-RAD biodistributions were similar with the exception of kidney and blood activities. ^{99m}Tc-RAFT-RGD activity in the infarcted area was significantly higher than that of ^{99m}Tc-RAFT-RAD, and the ^{99m}Tc-RAFT-RGD infarct-to-normal zone ratio by gamma-well counting was significantly higher than that of ^{99m}Tc-RAFT-RAD. The significant increase in ^{99m}Tc-RAFT-RAD activity in the ischemic and reperfused myocardium can likely be attributed to the presence of interstitial edema, as previously demonstrated by others[34] and as recently observed in our laboratory,[35] and to the observation that RAD-containing tracers may extravasate in the presence of an altered vascular permeability.[36] The ^{111}In-labeled, $\alpha_V\beta_3$ integrin-specific tracer ^{111}In-RP748 was recently evaluated by Meoli et al.[27] The authors demonstrated a nearly 2-fold increase in ^{111}In-RP748 activity in the previously ischemic and reperfused area by gamma-well counting, a value comparable to the 2.5-fold increase observed with ^{99m}Tc-RAFT-RGD in the present study.

Ex vivo imaging indicated a strong ^{99m}Tc-RAFT-RGD uptake in the peri-infarct and infarcted zones subjected to angiogenesis and strong $\alpha_V\beta_3$ expression with no uptake in the normal zone. The magnitude and extent of ^{99m}Tc-RAFT-RAD uptake both in the

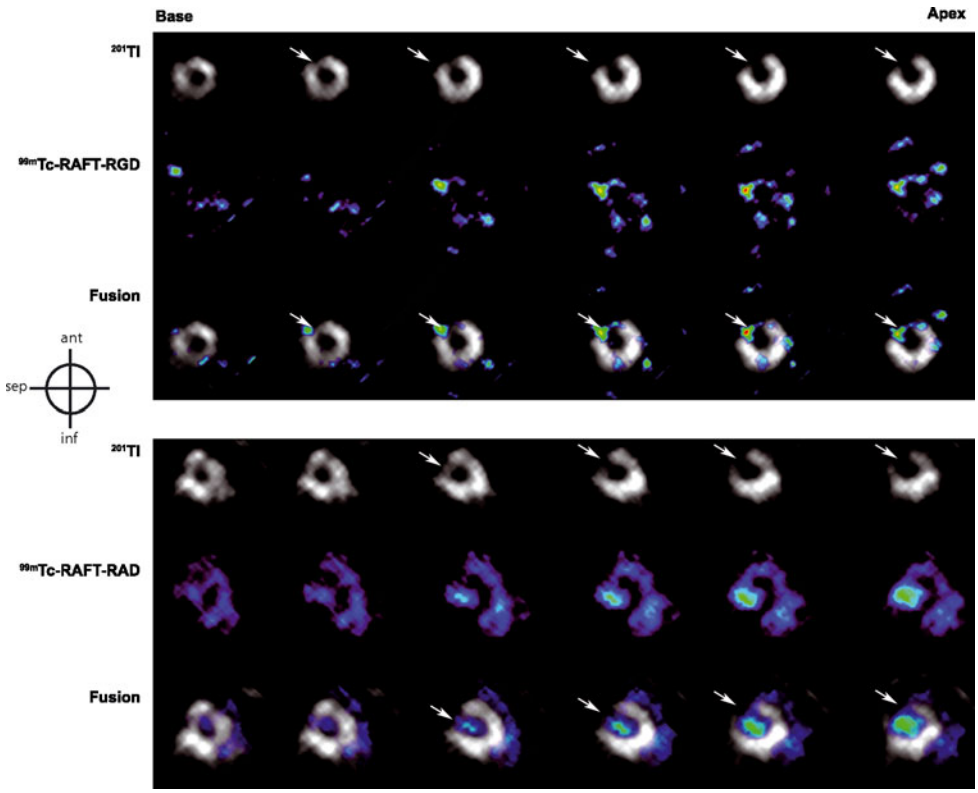

Figure 4. Representative ^{99m}Tc-RAFT-RGD and ^{99m}Tc-RAFT-RAD myocardial short axis images from base to apex with the corresponding ^{201}Tl perfusion as obtained by SPECT imaging. Note that there was a focal uptake of ^{99m}Tc-RAFT-RGD in the infarcted and reperfused area delineated by the ^{201}Tl perfusion defect whereas ^{99m}Tc-RAFT-RAD activity was mainly observed in the LV cavity.

peri-infarct and infarcted area was markedly lower than that of ^{99m}Tc-RAFT-RGD. ^{99m}Tc-RAFT-RGD infarct to normal ratio (4.9 ± 0.9) was comparable to what observed by Higuchi et al[30] using the PET tracer ^{18}F-Galacto-RGD 1 or 3 weeks following reperfusion in a similar model (3.4 ± 0.6 and 3.4 ± 0.9, respectively). Results from dual-isotope in vivo SPECT acquisitions indicated that ^{201}Tl images allowed the localization of the infarcted area characterized by a greater than 50% perfusion defect on short-axis images. Following ^{201}Tl and ^{99m}Tc image fusion, ^{99m}Tc-RAFT-RGD activity was readily observed in the infarcted area (mean infarct-to-normal zone ratio, 2.5 ± 0.6) whereas ^{99m}Tc-RAFT-RAD activity was mainly found in the left ventricular cavity, a result that is in accordance with the significantly higher blood activity of ^{99m}Tc-RAFT-RAD than ^{99m}Tc-RAFT-RGD (Table 1). For comparison, an infarct-to-normal zone tracer activity ratio of 1–1.6 has been obtained by Meoli et al following in vivo dual-isotope SPECT imaging of ^{111}In-RP748 and ^{99m}Tc-MIBI in a canine model of reperfused MI.[27] Lindsey et al[37] have successfully performed in vivo mouse SPECT imaging of perfusion and angiogenesis using ^{201}Tl and ^{99m}Tc-NC100692, respectively. However, in vivo image quantification was not performed, thereby not allowing a comparison with the results of the present study.

Limitations of the study First, immunohistochemical stainings were performed on dedicated animals, thereby limiting the power to directly correlate in vivo imaging with histological findings. Also, CD31 immunostaining identified mature capillary endothelial cells, which probably did not express integrins. However, integrin expression restricted to the infarcted and reperfused area was confirmed by direct $\alpha_v\beta_3$ immunohistochemical staining. Finally, sham-operated animals were not performed in the present study since control experiments consisted in the injection of the non-specific tracer ^{99m}Tc-RAFT-RAD. However, it is known that a number of modifications might occur in the remote, non-infarcted region of the myocardium over the course of reperfused MI.

In conclusion, ^{99m}Tc-RAFT-RGD allowed the non-invasive nuclear imaging of ischemia-reperfusion-induced myocardial angiogenesis. Further studies are warranted to determine the potential of ^{99m}Tc-RAFT-

RGD for the clinical imaging of angiogenesis, including sensitivity studies using pro- and anti-angiogenic therapies.

References

1. Cardiovascular Diseases. World Health Organization, fact sheet #317, 2007. Available at http://www.who.int/mediacentre/factsheets/fs317/en/index.html.
2. Lloyd-Jones D, Adams RJ, Brown TM, Carnethon M, Dai S, De Simone G, et al. Heart disease and stroke statistics—2010 update. A report from the American Heart Association. Circulation. 2009. [Epub ahead of print].
3. Sutton MG, Sharpe N. Left ventricular remodeling after myocardial infarction—pathophysiology and therapy. Circulation 2000;101:2981-8.
4. Gheorghiade M, Sopko G, De Luca L, Velazquez EJ, Parker JD, Binkley PF, et al. Navigating the crossroads of coronary artery disease and heart failure. Circulation 2006;114:1202-13.
5. Frangogiannis NG, Smithb CW, Entman ML. The inflammatory response in myocardial infarction. Cardiovasc Res 2002;53:31-47.
6. Tucker GC. Integrins: Molecular targets in cancer therapy. Curr Oncol Rep 2006;8:96-103.
7. Kocher AA, Schuster MD, Szabolcs MJ, Takuma S, Burkhoff D, Wang J, et al. Neovascularization of ischemic myocardium by human bone-marrow-derived angioblasts prevents cardiomyocyte apoptosis, reduces remodeling and improves cardiac function. Nat Med 2001;7:430-6.
8. Hao X, Mansson-Broberg A, Grinnemo KH, Siddiqui AJ, Dellgren G, Brodin LA, et al. Myocardial angiogenesis after plasmid or adenoviral VEGF-A(165) gene transfer in rat myocardial infarction model. Cardiovasc Res 2007;73:481-7.
9. Okazaki T, Ebihara S, Asada M, Yamanda S, Saijo Y, Shiraishi Y, et al. Macrophage colony-stimulating factor improves cardiac function after ischemic injury by inducing vascular endothelial growth factor production and survival of cardiomyocytes. Am J Pathol 2007;71:1093-103.
10. Chen LL, Yin H, Huang J. Inhibition of TGF-beta1 signaling by eNOS gene transfer improves ventricular remodeling after myocardial infarction through angiogenesis and reduction of apoptosis. Cardiovasc Pathol 2007;16:221-30.
11. Rafii S, Lyden D. Therapeutic stem and progenitor cell transplantation for organ vascularization and regeneration. Nat Med 2003;9:702-12.
12. Hughes GC, Biswas SS, Yin B, Coleman RE, DeGrado TR, Landolfo CK, et al. Therapeutic angiogenesis in chronically ischemic porcine myocardium: Comparative effects of bFGF and VEGF. Ann Thorac Surg 2004;77:812-8.
13. Simons M, Ware JA. Therapeutic angiogenesis in cardiovascular disease. Nat Rev Drug Discov 2003;2:863-71.
14. Koneru S, Penumathsa SV, Thirunavukkarasu M, Vidavalur R, Zhan L, Singal PK, et al. Sildenafil mediated neovascularization and protection against myocardial ischemia reperfusion injury in rats: Probable role of VEGF/angiopoietin-1. J Cell Mol Med 2008;12:2651-64.
15. Halkos ME, Zhao ZQ, Kerendi F, Wang NP, Jiang R, Schmarkey LS, et al. Intravenous infusion of mesenchymal stem cells enhances regional perfusion and improves ventricular function in a porcine model of myocardial infarction. Basic Res Cardiol 2008;103:525-36.
16. Yla-Herttuala S, Rissanen TT, Vajanto I, Hartikainen J. Vascular endothelial growth factors: Biology and current status of clinical applications in cardiovascular medicine. J Am Coll Cardiol 2007;49:1015-26.
17. Nordlie MA, Wold LE, Simkhovich BZ, Sesti C, Kloner RA. Molecular aspects of ischemic heart disease: Ischemia/reperfusion-induced genetic changes and potential applications of gene and RNA interference therapy. J Cardiovasc Pharmacol Ther 2006;11:17-30.
18. Sinusas AJ. Imaging of angiogenesis. J Nucl Cardiol 2004;11:617-33.
19. Brooks PC, Clark RA, Cheresh DA. Requirement of vascular integrin $\alpha_V\beta_3$ for angiogenesis. Science 1994;264:569-71.
20. Ruoslahti E. The RGD story: A personal account. Matrix Biol 2003;22:459-65.
21. Haubner R, Weber WA, Beer AJ, Vabuliene E, Reim D, Sarbia M, et al. Non-invasive visualization of the activated $\alpha_V\beta_3$ integrin in cancer patients by positron emission tomography and [18F]-galacto-RGD. PLoS Med 2005;2:244-52.
22. Fani M, Psimadas D, Zikos C, Xanthopoulos S, Loudos GK, Bouziotis P, et al. Comparative evaluation of linear and cyclic 99mTc-RGD peptides for targeting of integrins in tumor angiogenesis. Anticancer Res 2006;26:431-4.
23. Boturyn D, Coll JL, Garanger E, Favrot MC, Dumy P. Template assembled cyclopeptides as multimeric system for integrin targeting and endocytosis. J Am Chem Soc 2004;126:5730-9.
24. Sancey L, Ardisson V, Riou LM, Ahmadi M, Marti-Batlle D, Boturyn D, et al. In vivo imaging of tumour angiogenesis in mice with the alpha(v)beta (3) integrin-targeted tracer ^{99m}Tc-RAFT-RGD. Eur J Nucl Med Mol Imaging 2007;34:2037-47.
25. Sancey L, Garanger E, Foillard S, Schoehn G, Hurbin A, Albiges-Rizo C, et al. Clustering and internalization of integrin alphavbeta3 with a tetrameric RGD-synthetic peptide. Mol Ther 2009;17:837-43.
26. Makowski MR, Ebersberger U, Nekolla S, Schwaiger M. In vivo molecular imaging of angiogenesis, targeting alphavbeta3 integrin expression, in a patient after acute myocardial infarction. Eur Heart J 2008;29:2201.
27. Meoli DF, Sadeghi MM, Krassilnikova S, Bourke BN, Giordano FJ, Dione DP, et al. Noninvasive imaging of myocardial angiogenesis following experimental myocardial infarction. J Clin Invest 2004;113:1684-91.
28. Savill J, Dransfield I, Hogg N, Haslett C. Vitronectin receptor-mediated phagocytosis of cells undergoing apoptosis. Nature 1990;343:170-3.
29. Sun Y, Zhang JQ, Zhang J, Lamparter S. Cardiac remodeling by fibrous tissue after infarction in rats. J Lab Clin Med 2000;135:316-23.
30. Higuchi T, Bengel FM, Seidl S, Watzlowik P, Kessler H, Hegenloh R, et al. Assessment of avb3 integrin expression after myocardial infarction by positron emission tomography. Cardiovasc Res 2008;78:395-403.
31. Dijkgraaf I, Kruijtzer JA, Liu S, Soede AC, Oyen WJ, Corstens FH, et al. Improved targeting of the alpha(v)beta(3) integrin by multimerisation of RGD peptides. Eur J Nucl Med Mol Imaging 2007;34:267-73.
32. Garanger E, Boturyn D, Coll JL, Favrot MC, Dumy P. Multivalent RGD synthetic peptides as potent alphaVbeta3 integrin ligands. Org Biomol Chem 2006;4:1958-65.
33. Cheng YF, Kramer RH. Human microvascular endothelial cells express integrin-related complexes that mediate adhesion to the extracellular matrix. J Cell Physiol 1989;139:275-86.
34. Whalen DA, Hamilton DG, Ganote CE, Jennings RB. Effect of a transient period of ischemia on myocardial cells. I. Effects on cell volume regulation. Am J Pathol 1974;74:381-97.
35. Riou LM, Broisat A, Lartizien C, Toufektsian MC, Maitrejean S, Janier M, et al. Assessment of non-reperfused and reperfused

myocardial infarction using diffusible or deposited radiolabelled perfusion imaging agents. Eur J Nucl Med Mol Imaging 2007;34:330-7.

36. Mulder WJ, Strijkers GJ, Habets JW, Bleeker EJ, van der Schaft DW, Storm G, et al. MR molecular imaging and fluorescence microscopy for identification of activated tumor endothelium using a bimodal lipidic nanoparticle. FASEB J 2005;19:2008-10.
37. Lindsey ML, Escobar PG, Dobrucki LW, Goshorn DK, Bouges S, Mingoia JT, et al. Matrix metalloproteinase-9 gene deletion facilitates angiogenesis after myocardial infarction. Am J Physiol Heart Circ Physiol 2006;290:H232-9.